arXiv:1202.1716v1 [cond-mat.soft] 8 Feb 2012

Breakdown of the Amontons' Law of Friction in Elastic Object with Friction Obeying Amontons' Law Locally

Michio Otsuki and Hiroshi Matsukawa
Department of Physics and Mathematics, Aoyama Gakuin University, 5-10-1 Fuchinobe, Sagamihara 252-5258, Japan

(Dated: February 9, 2012)

We show that the Amontons' law of friction breaks down in the elastic object which has the friction force obeying the Amontons' law locally. By the finite element method, it is shown that the bulk static friction coefficient $\mu_{\rm M}$ decreases with increasing pressure and system length. It also depends on the apparent contact area. These behaviors indicate the breakdown of the Amontons' law and result from the local slip before the onset of bulk sliding. These results are consistent with experiments. An effective one-dimensional model well explains these behaviors analytically.

PACS numbers: 46.55.+d, 46.50.+a, 62.20.Qp, 81.40.Pq

In the 15th century da Vinci discovered that the resistance against the sliding motion of the solid object on substrate does not depend on the apparent contact area and is doubled if the load of the object is doubled [1, 2]. The discovery was rediscovered by Amontons about 200 years later and is now summarized by, the so-called, Amontons' law of friction: the friction force does not depend on the apparent contact area and is proportional to the loading force. The ratio of the friction force to the loading force is called the friction coefficient, which does not depend on the apparent contact area and the loading force. It is well known that the Amontons' law holds well for various systems. The law is usually explained as resulting from increase of the area of actual contact points, in which two surfaces actually contact each other via intermolecular forces, in proportion to the loading force [1, 2].

It is also well known, however, that the Amontons' law breaks down in some systems, e.g., the systems with large adhesion [1, 2]. Here, we show the breakdown of the Amontons' law in an elastic object by both of numerical and analytic methods. The object has the friction force obeying the Amontons' law locally and is under uniform pressure $P_{\rm ext}$ and pushed by the external shear force $F_{\rm T}$ from the trailing edge as shown in Fig. 1(a). Numerical analysis based on a 2D finite element method (FEM) shows that the bulk static friction coefficient $\mu_{\rm M}$, which corresponds to the onset of sliding of the whole object, decreases with increasing $P_{\rm ext}$. That indicates the breakdown of the Amontons' law and is consistent with experiments [3, 4]. The breakdown is closely related to the local slip also observed in experiments [5–8] and theoretical and numerical works [8–13]. The shear force $F_{\rm T}$ well below the bulk maximum static friction force induces a precursor, that is the local slip from the trailing edge of the object. The slip front proceeds slowly with slowly increasing $F_{\rm T}$. When the traveling length of the front reaches a critical length $\ell_{\rm c}$, the slow motion becomes unstable and changes to rapid motion. Then, the slip front quickly arrives at the trailing edge and the whole object slides. The magnitude of $\mu_{\rm M}$ depends on $\ell_{\rm c}$ as $\mu_{\rm M} \simeq \mu_{\rm K} + (\mu_{\rm S} - \mu_{\rm K})(\ell_{\rm c}/L)$, where $\mu_{\rm S}, \mu_{\rm K}$, and L are the local static and kinetic friction coefficients and the system length, respectively and $\mu_{\rm S} > \mu_{\rm K}$. The critical length $\ell_{\rm c}$ decreases with increasing $P_{\rm ext}$. Then, $\mu_{\rm M}$ decreases with increasing $P_{\rm ext}$. These behaviors are well explained analytically based on a 1D effective model.

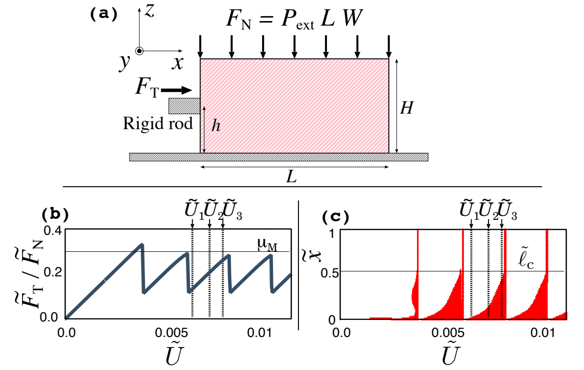

FIG. 1. (color online). (a) The elastic object is under uniform pressure $P_{\rm ext} = F_{\rm N}/(LW)$ and pushed at height h by a rigid rod with the shear force $F_{\rm T}$. (b) The ratio of the shear force to the loading force $\tilde{F}_{\rm T}/\tilde{F}_{\rm N}$ vs the displacement of the pushing rod $\tilde{U} = \tilde{V}\tilde{t}$ for $\tilde{L} = 1.0, d = 0.5, \tilde{P}_{\rm ext} = 0.0004$ and the parameter set (A). (c) The local slip region is shown by the gray area (the red area for online version) in the $\tilde{U} - \tilde{x}$ plane for the same parameters with those in (b). The horizontal line shows the critical traveling length of the slip front $\tilde{\ell}_{\rm c}$.

We first analyze the rectangular elastic object on a rigid substrate by FEM, which has length L, width W and height H along x, y, z-axes, respectively and mass density ρ. The plain stress condition is assumed along the $y-$axis. We apply the uniform pressure $P_{\rm ext} = F_{\rm N}/(LW)$ at the top surface, where $F_{\rm N}$ is the loading force, and the shear force $F_{\rm T}$ from the trailing edge at height h by a rigid rod. Hereafter, we set $W = 1$ and $h = H/2$. The equation of motion of the displacement vector of the elastic object $\boldsymbol{u}(\boldsymbol{r}, t)$ is expressed as $\rho\frac{\partial^2}{\partial t^2}\boldsymbol{u}(\boldsymbol{r}, t) = \boldsymbol{\nabla}\cdot\boldsymbol{\sigma}$ [14]. Here, $\boldsymbol{\sigma} = \boldsymbol{\sigma}^{\rm (el)} + \boldsymbol{\sigma}^{\rm (dis)}$ is the stress tensor composed from the elastic part $\boldsymbol{\sigma}^{\rm (el)}$ and the dissipation part $\boldsymbol{\sigma}^{\rm (dis)}$, of which (α, β) component is expressed as $\sigma^{\rm (dis)}_{\alpha\beta} = \eta_1\dot{\epsilon}_{\alpha\beta} + \eta_2(\dot{\epsilon}_{xx} + \dot{\epsilon}_{zz})\delta_{\alpha\beta}$. Here, $\dot{\epsilon}_{\alpha\beta}$ is the component of the strain rate tensor and η_1, η_2 are the viscosity coefficients. The boundary condition at the top surface is given by $\sigma_{zz} = -P_{\rm ext}$ and $\sigma_{xz} = 0$. The stress is free at $x = 0$ and L except at the rigid rod, which has width of $0.1H$ and moves with constant velocity V. The local friction force obeys the Amontons' law and gives the frictional stress, $\sigma_{xz}^{\rm fric} = \mu\,(\dot{u}_x)\,{\rm sign}(\dot{u}_x)|\sigma_{zz}|\theta(-\sigma_{zz})$, at the interface, where $\theta(x)$ is the Heaviside function [15]. The velocity v dependent friction coefficient $\mu(v)$ takes value from 0 to $\mu_{\rm S}$ at $v = 0$, decreases linearly from $\mu_{\rm S}$ to $\mu_{\rm K}$ for $0 \leq |v| \leq v_{\rm c}$, and equals to $\mu_{\rm K}$ for $v_{\rm c} \leq |v|$.

We introduce the normalized quantities in which the length, mass and time are normalized by $L_0 \equiv \eta_1/\sqrt{\rho E}$, $m_0 \equiv \eta_1^3/\sqrt{\rho E^3}$ and $t_0 \equiv \eta_1/E$, respectively, where E is the Young's modulus. We express normalized quantities with tilde. The model has parameters $\tilde{L} \equiv L/L_0, d \equiv H/L, \tilde{P}_{\rm ext} \equiv P_{\rm ext}/E, \tilde{V} \equiv Vt_0/L_0$, which characterize the sample size and the external condition, $\mu_{\rm S}, \mu_{\rm K}, \tilde{\eta}_2 \equiv \eta_2/\eta_1, \tilde{v}_c$, and the Poisson's ratio ν, which characterize the material properties. We employ two parameter sets: (A) simulates a model viscoelastic material, which has $\nu = 0.34, \mu_{\rm S} = 0.38, \mu_{\rm K} = 0.1, \tilde{v}_c = 3.4 \times 10^{-4}$, and $\tilde{\eta}_2 = 1$; (B) simulates polymethyl-methacrylate (PMMA), which has $\nu = 0.4, \mu_{\rm S} = 1.2, \mu_{\rm K} = 0.2, \tilde{v}_c = 3.9 \times 10^{-7}$, and $\tilde{\eta}_2 = 1$ [16]. In the FEM calculation, the object is divided into equal-size cells with rectangular shape. The number of cells is 40×40 or 80×80. The convergence of the results with respect to the number is verified. The following results are obtained for the limit of vanishing driving velocity.

In Fig. 1(b), we show the ratio of the shear force to the loading force $\tilde{F}_{\rm T}/\tilde{F}_{\rm N}$ as a function of the displacement of the pushing rod $\tilde{U} = \tilde{V}t$. At the beginning, we apply the uniform pressure at the top surface and make the elastic object relax. Then, we start pushing the object at $\tilde{t} = 0$. Periodic stick-slip motions are observed except the 1-st one, which is strongly influenced by the initial condition. Hereafter, we focus on the periodic regime. We define the bulk static friction coefficient $\mu_{\rm M}$ by the peak value of $\tilde{F}_{\rm T}/\tilde{F}_{\rm N}$. The pressure $\tilde{P}_{\rm ext}$ dependence of $\mu_{\rm M}$ is shown in Figs. 2(a,b) for the parameter set (A) and (B), respectively. It is to be noted that for PMMA, simulated by the parameter set (B), $\tilde{P}_{\rm ext} = 1.0 \times 10^{-4}$ and $\tilde{L} = 0.02$ correspond to $P_{\rm ext} = 3.0 \times 10^5$[Pa] and $L = 0.96$[m], respectively [17]. Clear decreases of $\mu_{\rm M}$ with increasing $\tilde{P}_{\rm ext}$ and $\tilde{L}$ are observed, which indicate the breakdowns of the Amontons' law and the extensive property of the friction force. Such pressure dependence is consistent with experiments of PMMA [3, 4]. It is well known that adhesion makes the friction coefficient increase with decreasing pressure [1, 2], but it does not exist in the present system. We show $\tilde{F}_{\rm N}$ dependence of $\mu_{\rm M}$ for the case laying the longer edge of a rectangular object on the substrate and that laying the shorter one in Fig. 2(c). The friction coefficient decreases with increasing $\tilde{F}_{\rm N}$ and depends on the apparent contact area, which also indicates the breakdown of the Amontons' law.

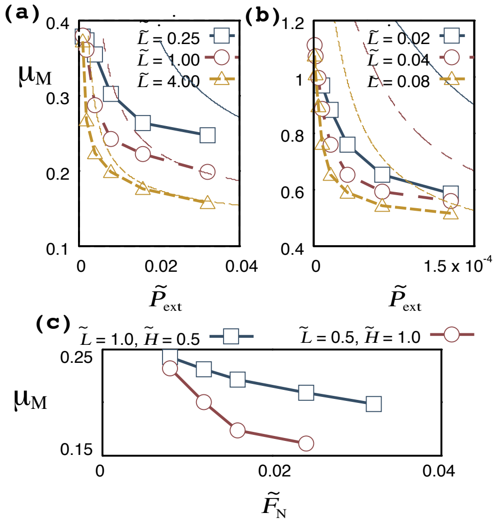

FIG. 2. (color online). The pressure $\tilde{P}_{\rm ext}$ dependence of $\mu_{\rm M}$ for the parameter set (A) (a) and (B) (b). The lines with symbols indicate the results of the FEM calculation. Thin lines indicate the analytic results based on the effective 1D model, where we set $\theta = 0.2$. The lines with the same type correspond to the same value of $\tilde{L}$. (c) The loading force $\tilde{F}_{\rm N}$ dependence of $\mu_{\rm M}$ for the case laying the longer edge of a rectangular object on the substrate ($\tilde{L} = 1.0, \tilde{H} = 0.5$) and that laying the shorter one ($\tilde{L} = 0.5, \tilde{H} = 1.0$) for the parameter set (A).

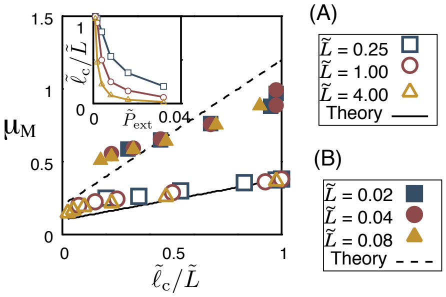

FIG. 3. (color online). The bulk friction coefficient $\mu_{\rm M}$ as a function of $\tilde{\ell}_{\rm c}/\tilde{L}$ for various values of $\tilde{P}_{\rm ext}$ and $\tilde{L}$ and for the parameter set (A) and (B). The lines show the theoretical result, Eq. (3). The inset shows the pressure $\tilde{P}_{\rm ext}$ dependence of $\tilde{\ell}_{\rm c}/\tilde{L}$ for $d = 0.5$ and the parameter set (A).

The change of $\mu_{\rm M}$ shown in Fig. 2 results from the local slip before the onset of bulk sliding also observed in experiments of PMMA [5–8]. In Fig. 1(c), we show the local slip region, where the velocity at the interface has a finite value, in the $\tilde{U} - \tilde{x}$ plane. The shear force $\tilde{F}_{\rm T}$ well below the bulk maximum static friction force induces slow local slip from the trailing edge. The slip front proceeds slowly and the traveling length of the front $\tilde{\ell}$ grows with $\tilde{U}$. When $\tilde{\ell}$ reaches the critical length $\tilde{\ell}_{\rm c}$, the front starts rapid motion, which accompanies rapid local slip. Then, the front enters the leading edge quickly, the whole object slides, and $F_{\rm T}$ drops sharply. These behaviors are consistent with experiments [6]. Further increase of $\tilde{U}$ repeats the similar behavior. Figure 3 shows that $\mu_{\rm M}$ is scaled by $\tilde{\ell}_{\rm c}/\tilde{L}$ for each parameter set. The scaling with

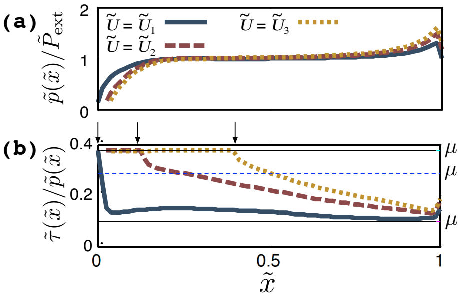

FIG. 4. (color online) The normalized pressure $\tilde{p}(\tilde{x})/\tilde{P}_{\rm ext}$ (a) and the ratio of the shear stress to the pressure $\tilde{\tau}(\tilde{x})/\tilde{p}(\tilde{x})$ (b) at the interface for the magnitudes of $\tilde{U}$ indicated by arrows in Figs. 1(b,c). The arrows in (b) indicate the position of the slip front. The horizontal lines indicate $\mu_{\rm S}, \mu_{\rm M}$, and $\mu_{\rm K}$. The parameters are same with those in Figs. 1(b,c).

the pressure $\tilde{P}_{\rm ext}$ dependence of $\tilde{\ell}_{\rm c}/\tilde{L}$ shown in the inset of Fig. 3 gives the $\tilde{P}_{\rm ext}$ dependence of $\mu_{\rm M}$.

We show the pressure at the interface $\tilde{p}(\tilde{x}) \equiv -\tilde{\sigma}_{zz}|_{\tilde{z}=0}$ in Fig. 4(a) for the magnitudes of $\tilde{U}$ indicated by arrows in Figs. 1(a,b). The applied pressure at the top surface is uniform, but $\tilde{p}(\tilde{x})$ depends strongly on $\tilde{x}$ and increases with $\tilde{x}$. Similar pressure distribution is observed in experiments [4, 7] and results from the torque induced by the shear force $\tilde{F}_{\rm T}$ [9]. The low pressure at the trailing edge makes the local maximum static friction force small. As a result, the local slip starts from there. Figure 4(b) shows the ratio of the shear stress at the interface $\tilde{\tau}(\tilde{x}) \equiv \tilde{\sigma}_{xz}|_{\tilde{z}=0}$ to the pressure, $\tilde{\tau}(\tilde{x})/\tilde{p}(\tilde{x})$. Just after the sliding of the whole object, which accompanies rapid slip in the entire interface, the ratio is approximately equals to $\mu_{\rm K}$ (dashed line). The reason is considered as follows. During the acceleration of the rapid slip of any portion in the interface, the local friction coefficient there decreases to $\mu_{\rm K}$. At the instance of vanishing acceleration, the local shear stress at the interface $\tilde{\tau}(\tilde{x})$ is equal to the local frictional stress $\mu_{\rm K}\tilde{p}(\tilde{x})$. Then, the portion decelerate and the local friction coefficient rapidly approaches to $\mu_{\rm S}$. When the portion stops slip, however, $\tilde{\tau}(\tilde{x})$ keeps the magnitude $\mu_{\rm K}\tilde{p}(\tilde{x})$ due to finite relaxation time. Finally, the local frictional stress after the rapid sliding of the whole object relaxes to $\mu_{\rm K}\tilde{p}(\tilde{x})$. By contrast, in the region where the slow local slip has occurred, the figure shows that the ratio $\tilde{\tau}(\tilde{x})/\tilde{p}(\tilde{x})$ equals to $\mu_{\rm S}$ because $\tilde{\tau}(\tilde{x})$ is given by the local frictional stress for vanishing velocity $\mu_{\rm S}\tilde{p}(\tilde{x})$ after the slow slip [18]. Figure 4(b) also shows that the local magnitude of $\tilde{\tau}(\tilde{x})/\tilde{p}(\tilde{x})$ can be larger than the bulk frictional coefficient $\mu_{\rm M}$ without precipitating the local slip as observed in experiments [4, 7]. The bulk maximum static friction coefficient $\mu_{\rm M}$ is then determined at the onset of rapid motion of the local slip front, which is also shown analytically below.

In order to analyze the transition from the slow to rapid motions of the local slip front at $\tilde{\ell}_{\rm c}$, we employ an effective 1D model, in which the degrees of freedom of the elastic object along the z-axis are neglected. The equation of motion of the model is expressed as,

$$\frac{\partial^2 \tilde{u}(\tilde{x},\tilde{t})}{\partial \tilde{t}^2} = \frac{\partial \tilde{\sigma}_{xx}(\tilde{x},\tilde{t})}{\partial \tilde{x}} + \frac{\tilde{\sigma}_{xz}(\tilde{x},\tilde{t}) - \tilde{\sigma}_{xz}^{\rm (fric)}}{\theta \tilde{H}}. \tag{1}$$

Here, $\tilde{u}(\tilde{x},\tilde{t})$ is the displacement along the x-axis at the interface, and $\theta\tilde{H}$ is the characteristic length of the variation of the (xz) component of the stress. Here, we employ θ as a fitting parameter. The shear stress is given by $\tilde{\sigma}_{xx} = \tilde{E}_1 \frac{\partial \tilde{u}}{\partial \tilde{x}} + \tilde{\eta}_t \frac{\partial^2 \tilde{u}}{\partial \tilde{x} \partial \tilde{t}}$, $\tilde{\sigma}_{xz} = \tilde{E}_2 \frac{\tilde{U}-\tilde{u}}{\tilde{h}} + \frac{1}{2\tilde{h}}(\tilde{V} - \frac{\partial}{\partial \tilde{t}}\tilde{u})$, where $\tilde{\eta}_t \equiv 1 + \tilde{\eta}_2$. The frictional stress $\tilde{\sigma}_{xz}^{\rm (fric)}$ is given as before and $\tilde{E}_1 \equiv 1/\{(1+\nu)(1-\nu)\}, \tilde{E}_2 \equiv 1/\{2(1+\nu)\}$. We assume that the pressure at the interface is given by $\tilde{p}(\tilde{x}) = 2\tilde{P}_{\rm ext}\tilde{x}/\tilde{L}$, which simulates the result shown in Fig. 4(a). The boundary condition is given by $\frac{\partial}{\partial \tilde{x}}\tilde{u}(\tilde{x},\tilde{t}) = 0$ at $\tilde{x} = 0$ and $\tilde{L}$. Hereafter, we set the origin of $\tilde{U}$ to the position of the pushing rod just after the sliding of the whole object. The adiabatic solution of Eq. (1) for $\tilde{U} = 0$ is obtained as

$$\tilde{u}_0(\tilde{x}) = \frac{2\mu_{\rm K}\tilde{h}\tilde{P}_{\rm ext}}{\tilde{E}_2\tilde{L}} \Big\{ \frac{\kappa\tilde{r}}{\sinh\frac{\tilde{L}}{\kappa\tilde{r}}} \big(\cosh\frac{\tilde{x}}{\kappa\tilde{r}} - \cosh\frac{\tilde{L}-\tilde{x}}{\kappa\tilde{r}} \big) - \tilde{x} \Big\},$$

where $\kappa^2 \equiv \tilde{E}_1/\tilde{E}_2$ and $\tilde{r}^2 \equiv \theta\tilde{h}\tilde{H}$. Here, we set the local friction coefficient to $\mu_{\rm K}$ as discussed before. For $\tilde{U} > 0$, the local slip front proceeds to $\tilde{\ell}$. The adiabatic solution for $\tilde{U} > 0$ is expressed as

$$\tilde{u}_{\rm a}(\tilde{x}) = \begin{cases} \tilde{u}_1(\tilde{x}), & 0 \le \tilde{x} \le \tilde{\ell}, \\ \tilde{u}_0(\tilde{x}), & \tilde{\ell} \le \tilde{x}. \end{cases} \tag{2}$$

The value of $\tilde{u}_{\rm a}(x)$ and its derivative must be continuous at $\tilde{x} = \tilde{\ell}$. In the region $\tilde{\ell} < \tilde{x}$, the increase of the shear stress with increasing $\tilde{U}$ is cancelled by the increase of the local frictional stress, which takes value between $\mu_{\rm K}\tilde{p}(\tilde{x})$ and $\mu_{\rm S}\tilde{p}(\tilde{x})$. The solution is then given by $\tilde{u}_0(\tilde{x})$. The solution in the region $0 \le \tilde{x} \le \tilde{\ell}$, where the local friction coefficient is equal to $\mu_{\rm S}$, is obtained as,

$$\begin{aligned} \tilde{u}_1(\tilde{x}) &= \tilde{u}_0(\tilde{x}) + \tilde{U}\big(1 - \cosh\frac{\tilde{x}-\tilde{\ell}}{\kappa\tilde{r}}\big) \\ &+ \frac{2(\mu_{\rm S}-\mu_{\rm K})\tilde{h}\tilde{P}_{\rm ext}}{\tilde{E}_2\tilde{L}} \Big\{ \ell\cosh\frac{\tilde{\ell}-\tilde{x}}{\kappa\tilde{r}} - \kappa\tilde{r}\sinh\frac{\tilde{\ell}-\tilde{x}}{\kappa\tilde{r}} - \tilde{x} \Big\}. \end{aligned}$$

The boundary condition at $\tilde{x} = 0$ gives $\tilde{\ell} \simeq \tilde{E}_2\tilde{L}\tilde{U}/\{(\mu_{\rm S}-\mu_{\rm K})\tilde{h}\tilde{P}_{\rm ext}\}$ for $\tilde{\ell}/\tilde{L} \ll 1$. Hence, $\tilde{\ell}$ grows adiabatically with adiabatic increase of $\tilde{U}$ as shown in the FEM calculation Fig. 1(c). Similar result is obtained based on a 1D spring-block model [13]. When $\tilde{\ell}$ reaches the the critical length $\tilde{\ell}_{\rm c}$, the adiabatic motion becomes unstable and changes to rapid motion. Then, the whole object slides. Employing the adiabatic equation, substituting the relation between $\tilde{U}$ and $\tilde{\ell}$, and setting $\tilde{\ell} = \tilde{\ell}_{\rm c}$ in the expression of the shear force $\tilde{F}_{\rm T} = \int_0^{\tilde{L}} d\tilde{x}\tilde{\sigma}_{xz}(\tilde{x})$, we get

$$\mu_{\rm M} = \mu_{\rm K} + (\mu_{\rm S} - \mu_{\rm K})\frac{\tilde{\ell}_{\rm c}}{\tilde{L}}. \tag{3}$$

for $\tilde{\ell}_{\rm c}/\tilde{L} \ll 1$. This relation agrees well with the FEM calculation as shown in Fig. 3 even for $\tilde{\ell}_{\rm c}/\tilde{L} \lesssim 1$.

The critical length $\tilde{\ell}_{\rm c}$ is given by the linear stability analysis of Eq. (1) in the limit of vanishing driving velocity $\tilde{V}$. Setting $\tilde{u}(\tilde{x},\tilde{t}) = \tilde{u}_a(\tilde{x}) + \delta\tilde{u}(\tilde{x},\tilde{t})$ and linearizing Eq. (1) with respect to $\delta\tilde{u}(\tilde{x},\tilde{t})$, we obtain its time evolution equation. The boundary condition is given by $\frac{\partial}{\partial\tilde{x}}\delta\tilde{u}(\tilde{x},\tilde{t})|_{\tilde{x}=0} = 0$ and $\delta\tilde{u}(\tilde{x} > \tilde{\ell},\tilde{t}) = 0$. We express $\delta\tilde{u}(\tilde{x},\tilde{t}) = \sum_{m=0} \tilde{u}_m \exp(\omega_m\tilde{t})\cos(k_m\tilde{x}/\tilde{\ell})$, where $\tilde{k}_m = (2m+1)\pi/2$. The time evolution equation gives

$$\omega_n^2 + \Big(\tilde{\eta}_t\frac{k_n^2}{\tilde{\ell}^2} + \frac{1}{2\tilde{r}^2}\Big)\omega_n + \tilde{E}_1\Big(\frac{k_n^2}{\tilde{\ell}^2} + \frac{1}{\kappa^2\tilde{r}^2}\Big) - \frac{(\mu_{\rm S}-\mu_{\rm K})\tilde{P}_{\rm ext}\tilde{\ell}}{\tilde{v}_{\rm c}\theta\tilde{H}\tilde{L}}\Big(1-\frac{1}{k_n^2}\Big)\omega_n = 0. \tag{4}$$

Here, off-diagonal terms are neglected, which are higher order of $\tilde{\ell}$. The eigenvalue ω_n gives the instability condition of $\tilde{u}_{\rm a}$. Usually, the instability results from the appearance of positive real part of any eigenvalue. In the present case, however, the backward motion of the fluctuation $\delta\tilde{u}$ is inhibited because it relaxes the local shear stress and the frictional stress stops it. That means the oscillating fluctuation never grows. The appearance of positive eigenvalue results in the instability. For the case of small value of $\tilde{P}_{\rm ext}$ or $\tilde{\ell}$, the viscosity in the 2nd term in Eq. (4) stabilizes the adiabatic motion, but in the opposite case the velocity weakening friction force expressed by the last term leads to the instability. The instability occurs in the $n = 0$ mode at first and gives the relation between the critical length $\tilde{\ell}_{\rm c}$ and $\tilde{P}_{\rm ext}$ as

$$\tilde{P}_{\rm ext} = \frac{\pi^2}{\pi^2-4}\frac{\tilde{v}_{\rm c}\theta d}{(\mu_{\rm S}-\mu_{\rm K})}\frac{1}{\tilde{\ell}_{\rm c}} \times \left\{\tilde{\eta}_t\Big(\frac{\pi\tilde{L}}{2\tilde{\ell}_{\rm c}}\Big)^2 + \frac{1}{\theta d^2} + 2\tilde{L}\sqrt{\tilde{E}_1\Big(\frac{\pi\tilde{L}}{2\tilde{\ell}_{\rm c}}\Big)^2 + \frac{2\tilde{E}_2}{\theta d^2}}\right\}. \tag{5}$$

This equation gives $\tilde{\ell}_{\rm c}/\tilde{L}$ decreasing with increasing $\tilde{P}_{\rm ext}$ and $\tilde{L}$: for $\tilde{\ell}_{\rm c}/\tilde{L} \ll 1$, $\tilde{\ell}_{\rm c}/\tilde{L} \propto (\tilde{L}\tilde{P}_{\rm ext})^{-1/3}$. That is consistent with the FEM calculation shown in the inset of Fig. 3. The function $\tilde{\ell}_{\rm c}(\tilde{P}_{\rm ext},\tilde{L})$ is given by Eq. (5) implicitly. By putting $\tilde{\ell}_{\rm c}$ into Eq. (3), we obtain the pressure and system length dependences of the friction coefficient $\mu_{\rm M}$. The results are shown in Figs. 2(a,b). The analytical results agree with the FEM calculation semiquantitatively for parameter set (A) and qualitatively for (B).

In conclusion, we show that the bulk static friction coefficient $\mu_{\rm M}$ of the elastic object decreases with increasing pressure and system length, which is consistent with experiments [3, 4]. The magnitude of $\mu_{\rm M}$ also depends on the apparent contact area. These behaviors have strong relation with the transition from slow to rapid motions of the local slip front. For large or small enough pressure and/or system length, where the ratio of the critical length of the transition to the system length is much less than or approximately equals to unity, $\mu_{\rm M}$ becomes constant and the Amonton's law holds. The present result may give a new method to control friction.

The authors thank to J. Fineberg, K. Nakano, M. O. Robbins, and T. Yamaguchi for valuable discussions. This work was supported by KAKENHI (22540398) and (22740260) and by HAITEKU from MEXT.

---

[1] B. N. J. Persson, *Sliding Friction -Physical Principles and Applications-*, 2nd ed. (Springer, Berlin, 2000).

[2] V. L. Popov, *Contact Mechanics and Friction -Physical Principles and Applications-*, (Springer, Berlin, 2010).

[3] S. Bouissou, J. Petit, and M. Barquins, Wear **214**, 156 (1998).

[4] O. Ben-David and J. Fineberg, Phys. Rev. Lett. **106**, 254301 (2011).

[5] S. M. Rubinstein, G. Cohen, and J. Fineberg, Nature **430**, 1055 (2004).

[6] S. M. Rubinstein, G. Cohen, and J. Fineberg, Phys. Rev. Lett. **98**, 226103 (2007).

[7] O. Ben-David, G. Cohen, and J. Fineberg, Science **330**, 211 (2010).

[8] S. Maegawa, A. Suzuki, and K. Nakano, Tribol. Lett. **38**, 313 (2010).

[9] J. Scheibert and D. K. Dysthe, Europhys. Lett. **92**, 54001 (2010).

[10] J. Trømborg, J. Scheibert, D. S. Amundsen, K. Thøgersen, and A. Malthe-Sørenssen, Phys. Rev. Lett. **107**, 074301 (2011)

[11] O. M. Braun, I. Barel, and M. Urbakh, Phys. Rev. Lett. **103**, 194301 (2009).

[12] E. Bouchbinder, E. A. Brener, I. Barel, and M. Urbakh, Phys. Rev. Lett. **107**, 235501 (2011).

[13] D. S. Amundsen *et al.*, Tribol. Lett. **45**, 357 (2012).

[14] L. D. Landau and E.M. Lifshitz, *Theory of Elasticity*, 3rd ed. (Butterworth-Heinemann, Oxford, 1986).

[15] The resolution of the models considered here is larger than the mean distance between actual contact points and smaller than the length scale of the spatial variation of the pressure discussed below. The validity of the Amontons' law in this length scale for PMMA is supported by the proportionality of the actual contact area to the loading force observed by J. H. Diertich and B. D. Kilgore (Tectonophysics, **256**, 219 (1996)).

[16] We estimate $\mu_{\rm S}$ and $\mu_{\rm K}$ for PMMA from max. and min. values of the ratio of the local shear stress to the pressure in Figs. 4(b, c) in Ref. [4], respectively. The value of $v_{\rm c}$ is estimated from the values of $\mu_{\rm S}, \mu_{\rm K}$ and the linear fit of the steady state velocity dependence of the rate and state dependent friction law reported by T. Baumberger, P. Berthoud, and C. Caroli (Phys. Rev B **60**, 3928 (1999)).

[17] We estimate L_0 for PMMA as follows. In Ref. [4], $\mu_{\rm M} = 0.6$ for $L = 0.2$[m], $d = 0.5$, and $P_{\rm ext} = 1.67\times10^6$[Pa]. The FEM calculation gives $\mu_{\rm M} = 0.6$ for $\tilde{P}_{\rm ext}\tilde{L} = 2.3\times10^{-6}$. Then, we get $L_0 = 48$[m].

[18] In Ref. [10], numerical analysis of a spring-block model shows $\tilde{\tau}(\tilde{x})$ after the local slip is close to $\mu_{\rm K}\tilde{p}(\tilde{x})$ because the local friction in the limit of vanishing velocity is equal to $\mu_{\rm K}$ in that work, which differs from the present one.